

Research Paper

Cite this article: El Hajjaji C, Delhote N, Verdeyme S, Piechowiak M, Boyer L, Durand O (2021). Optimization of the conductivity of microwave components printed by inkjet and aerosol jet on polymeric substrates by IPL and laser sintering. *International Journal of Microwave and Wireless Technologies* **13**, 652–662. <https://doi.org/10.1017/S175907872100043X>

Received: 1 November 2020
Revised: 26 February 2021
Accepted: 4 March 2021
First published online: 16 April 2021



Key words:

IPL sintering; Laser sintering; Electrical conductivity; Passive components

Author for correspondence:

Chaimaa El Hajjaji,
E-mail: elhajjaji@xlim.fr

Optimization of the conductivity of microwave components printed by inkjet and aerosol jet on polymeric substrates by IPL and laser sintering

Chaimaa El Hajjaji¹ , Nicolas Delhote¹ , Serge Verdeyme¹,
Malgorzata Piechowiak², Laurence Boyer² and Olivier Durand²

¹CNRS-XLIM, UMR 7252, Limoges, France and ²CTTC Centre for Technology Transfers in Ceramics, Limoges, France

Abstract

In this work, microwave planar resonators are printed with silver nanoparticle inks using two printing technologies, inkjet printing and aerosol jet printing, on polyimide substrates. The microwave resonators used in this paper operate in the frequency band 5–21 GHz. The printing parameters, such as the number of printed layers of silver nanoparticle inks, drop spacing, and sintering time, were optimized to ensure repeatable and conductive test patterns. To improve the electrical conductivity of silver deposits, which are first dried using a hot plate or an oven, two complementary sintering methods are used: intense pulsed light (IPL) and laser sintering. This paper presents the results of different strategies for increasing the final quality factor of printed planar resonators and the trade-offs (sintering time versus final conductivity/unloaded Q) that can be reached. Improvement of the resonator unloaded quality factor (up to +55%) and of the equivalent electrical conductivity (up to 14.94 S/ μm) at 14 GHz have been obtained thanks to these nonconventional sintering techniques. The total sintering durations of different combinations of sintering techniques (hot plate, oven, IPL, and laser) range from 960 to 90 min with a final conductivity from 14.94 to 7.1 S/ μm at 14 GHz, respectively.

Introduction

In the past few years, several emerging technologies have been developed, such as inkjet printing (IJP), aerosol jet printing (AJP), screen printing, spray printing, nScript, and gravure printing. [1, 2]. Recently, interesting research has been performed using technologies such as IJP and AJP based on the direct writing approach, allowing noncontact deposition [3] on rigid (glass, alumina, Poly-Ether-Ether-Ketone (PEEK), etc.) or flexible (polyethylene terephthalate (PET), polyimide (PI), paper, etc.) substrates [4]. These technologies have become increasingly present in different fields (medical, photovoltaic, electronics, smart systems, aeronautics, etc.) [5]. These printing techniques are based on Computer Aided Design (CAD) manufacturing approaches [3], which start from the generation of digital files to the printing of samples by depositing metal layers without taking a mask manufacturing step (such as in conventional photolithography) [6].

IJP is a technology used for depositing thin layers on planar supports. It is widely used in the field of printed electronics [7, 8]. Because of its maturity, quick prototyping, versatility, and low cost, IJP technology is the most widely used printing technology in the industry [8, 9].

The high resolution of AJP allows the printing of millimetric components on planar or 3D supports (inclined, half sphere, slope, etc.) [10] and reaches sub-millimetric frequencies [10, 11] to satisfy the most demanding fields, such as aerospace and defence telecommunication applications.

Electronic components are printed by using printing technologies based on metallic nanoparticle inks, such as silver [12], gold [10, 13], and copper [14]. In the field of electronics, these inks are most commonly used because of their ease of formulation and good electrical properties. Because of the low cost and good conductivity of copper (bulk conductivity: 59 S/ μm) [15], it is a good option, but its high oxidation rate in ambient air and lower maturity have greatly reduced interest in this type of ink in terms of engineering [16]. However, being cheaper than gold and more thermodynamically stable than copper, silver inks with good dispersion, maturity, and excellent conductivity (bulk conductivity: 63 S/ μm) [15] have become an easy choice for printed electronics [10].

Sintering technologies are increasingly used in industry because of their importance in the military field and automotive sector. At one time, sintering was also used for the production of technical ceramics for electronics and the medical field.

© The Author(s), 2021. Published by Cambridge University Press in association with the European Microwave Association. This is an Open Access article, distributed under the terms of the Creative Commons Attribution licence (<http://creativecommons.org/licenses/by/4.0/>), which permits unrestricted re-use, distribution, and reproduction in any medium, provided the original work is properly cited.

Especially in the field of printed electronics, heat treatment is subdivided into two steps. The first step is drying to evaporate the organic substances present in the different inks (solvents, binders, anti-caking agents, etc.) [17]. The second step is sintering, which is crucial for the coalescence between the metal particles to improve the cohesion of the metal deposit and thus obtain good effective conductivity of the deposit [18].

Conventional heat treatment is generally used for resistant substrates with high glass transition temperatures (alumina, Rogers, glass, etc.) that can last for hours and reach high sintering temperatures of up to 1000°C for ceramics, for example [19].

Andrievski has shown that for identical thermal cycles, the decrease in particle size allows a reduction in the sintering starting temperature, which improves the densification kinetics and results in a higher relative density according to the temperature [11, 19]. This Herring similarity law shows the dependence of the particle size on the sintering temperature. A more detailed dependence is shown in [20]. Because of the nanometric size of the metal particles, the sintering temperature has been drastically reduced, which represents a transformation in the field of printed electronics. At lower thermal sintering temperatures (200°C) than usual, the electrical conductivity of the metal deposit can reach 20 S/μm and higher without damage to the metal layer or the substrate used [10].

In recent years, the development of printed electronics using polymer substrates has attracted considerable attention due to the potential of flexible and low-cost electronic devices. The limiting factor of the most commonly used polymer substrates is their low glass transition temperatures (T_g (PLA) = 60°C, T_g (PET) = 70°C, T_g (Acrylonitrile Butadiene Styrene (ABS)) = 110°C, T_g (Polyethylene Naphthalate (PEN)) = 120°C, etc.) [21, 22]. After metallization of polymer substrates, alternatives to high-temperature heat treatment will be used to improve the electrical conductivity of the metal deposits.

To solve the constraints related to the sintering of metallic nanoparticle inks on a flexible support, a large community of researchers and industrialists are interested in the development of new, selective sintering technologies. These technologies are mainly based on the concept of sintering only the ink while minimizing the thermal effect with the substrate. We can mention plasma sintering, fast electrical sintering, and sintering using electromagnetic excitation (infrared, laser, and photonic sintering by intense pulsed light (IPL)) [23].

The most commonly used treatments that give relevant results are laser sintering and sintering using short pulses of light, often called intense pulsed light sintering (IPL). The first treatment consists of scanning the laser near or on the metal layers [24] to densify the metal deposit locally and improve electrical conductivity.

The second treatment is based on the absorption by the metallic ink of light intensity and its conversion into thermal energy. Light is generated by xenon stroboscopic lamps with a wide emission spectrum. The light intensity is mainly localized in the visible range and corresponds well with the absorption of metallic nanoparticle inks.

In the state of the art, metallic deposits printed by additive technologies (IJP) with average thicknesses of 0.35 μm on polymer substrates (PET) and treated by laser sintering have DC electrical conductivities between 4.7 S/μm [25] and 10.4 S/μm [26].

For metal deposits printed by IJP with thicknesses between 1 and 10 μm on PI, the DC electrical conductivities are between 1.2 S/μm [27] and 21 S/μm [28].

PI is a flexible polymer substrate that is attracting the attention of researchers in several fields because of its excellent mechanical properties and good flexibility, chemical resistance, and electrical properties [29, 30]. Its high glass transition temperature and thermal resistance (T_g (PI) = 270°C) [22] makes it an excellent competitor, particularly in low-cost flexible electronics. For silver deposits printed by direct writing technologies on PI substrates and heat-treated at temperatures between 150 and 220°C, the DC electrical conductivity varies between 22 and 25 S/μm [27, 28].

Most of the literature has focused on DC electrical conductivity without providing information on the equivalent electrical conductivity as a function of microwave frequencies, which represents a limiting point for microwave applications.

In this paper, to optimize the performances of microwave planar filters dedicated to demanding applications, such as aerospace and defence, we propose to focus on direct printing technologies with silver ink (IJP and AJP). Standard planar ring resonators that operate in the frequency band (5–21 GHz) on a PI substrate have been selected as a representative resonator for these applications.

Our research will focus in particular on the improvement of the quality factor of this type of planar resonator using alternative treatment technologies (IPL and laser). This work will be based on three main axes. The first axis quantifies the improvement of the quality factor of these planar resonators during the treatment. The second axis consists of improving the ratio between the total treatment time and the quality factor of the planar resonators. Finally, the last axis presents the technique of extraction of the equivalent conductivity of the metallic deposit at different microwave frequencies, which represents one of the particularities of our paper.

This paper is subdivided into two main sections:

The first section will describe the microwave sample used for our research (planar microwave resonator), as well as the alternative sintering by IPL or laser and the microwave conductivity extraction technique. Illustrations by SEM (scanning electron microscope) and microscopic images of the metal layer after each IPL or laser treatment are also provided. The second section summarizes the results after IPL and laser sintering and the trade-off between conductive deposition and reduced processing time.

An earlier version of this paper was presented at the EuMW2020 conference and was published in its Proceedings [31]. In this extended version, two additional IPL processing parameters are presented accompanied by SEM images of a sectional view of the metal deposit. A new laser processing technology accompanied by SEM images before and after sintering is also added and compared to a previous work proposed at the EuMW2019 conference [32]. All the mentioned results are summarized in this paper along with the technological parameters and general recommendations needed to reproduce them.

Experiments

IPL sintering

IPL sintering consists of using an extremely powerful flash lamp with a broad and adjustable spectrum, including infrared, visible, and ultraviolet (UV) light. It sends intense, short pulses of light that are converted into heat to fuse ceramic or metal particles at room temperature without damaging substrates, which are often heat-sensitive (paper, cloth, plastic, thermoplastic, etc.). This treatment technique saves time and can homogeneously

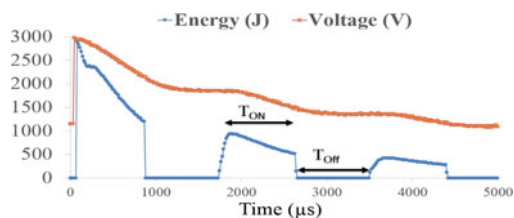


Fig. 1. Typical profile of the light pulses.

sinter a metal surface, particularly over large areas. This new technique was developed by NovaCentrix in 2006, but it remains less widespread than other sintering technologies for microwave applications.

The sintering equipment used in this work is a Xenon X-1100 IPL system that generates precisely controlled light pulses of high intensity. This system is presented in [31] with more details. Notably, the system cannot deliver the same energy for each light pulse. A typical profile of the train of pulses is shown in Fig. 1. The number of pulses can be selected, as well as their duration (T_{ON}) and the time between two pulses (T_{OFF}).

The IPL sintering system consists of the following components: a xenon flash lamp, a reflector, a UV filter, a power supply, capacitors, and a simmer triggering pulse controller. IPL is produced by a plasma arc between the electrodes after the gas is ionized by a voltage bias of 10 kV [33]. When the lamp is triggered using a pulse controller, ~ 1000 A of electrical current is delivered in a few milliseconds from the capacitor.

The optical spectrum of the light of our xenon lamp ranges in wavelength from 190 to 1100 nm. Because UV light degrades polymer substrates, a UV filter has been used to eliminate wavelengths below 380 nm [34]. Figure 1 represents the real shape of the pulses sent by the xenon lamp. For this example, the capacitor has been charged by a voltage of 3000 V, and the lamp sends three pulses of identical duration ($T_{ON} = T_{OFF} = 875$ μ s). As shown, the pulses and the voltage at the terminals of the capacitor follow the same decreasing tendency, which is explained in terms of the discharge of the capacitor.

Processing of inkjet-printed samples dried on a hot plate

Based on the work of Rojas-Nastrucci [35], a planar ring resonator was used to characterize the conductivity of the printed metal layer.

The samples are square ring resonators printed by IJP technology, as shown in Fig. 2(a), and are 2 mm long and 226 μ m wide ($W_{resonator}$). Their internal diameter (d_{in}) is 6.65 mm to have three resonances at ~ 7 , 14, and 21 GHz, as shown in Fig. 2(b). On a 125 μ m thick PI substrate, a silver metal layer of 1.6 μ m

thickness was deposited (average value). The resonator is excited by a microstrip line of 50 Ω , and finally, a coplanar to microstrip transition is used for GSG (ground–signal–ground) probe measurements of its S parameters. After printing, the samples were dried (before photonic sintering) on a hot plate at 200°C for 90 min to evaporate the solvents that were initially in the silver ink. Figure 2(c) shows a thermal image of the resonators during drying. The difference in colours on the plate proves the inhomogeneity of this sintering technique, which leads to slightly different quality factors for the different resonators. After drying on the hot plate for 90 min at 200°C, the unloaded quality factors of the resonators are between 11 and 16. The equivalent microwave conductivities are between 2.8 and 4.5 S/ μ m at 14 GHz, and the average continuous (DC) conductivity is 3.5 S/ μ m [7]. The samples will then be sintered with IPL.

Characterization of the printed ink conductivity. The PI substrate was precisely characterized using a resonant cavity method at three frequencies, and its properties are presented in Table 1.

The resonant ring presented in part A.1 is used to characterize the equivalent electrical conductivity of the printed metal layer at microwave frequencies. For conductivities from 3.5 to 40 S/ μ m, the quality factor value was calculated at three resonance frequencies (7, 14, and 21 GHz). The results obtained by the simulation with HFSS (high frequency structure simulator) are presented in Fig. 3. Figure 3(a) shows that the improvement of the conductivity leads to higher S_{21} peak values and to a slight shift of the resonance frequencies of the ring resonator. This behavior is expected in the following measurements. The plot of the values of the simulated quality factors (Fig. 3(b)) allows the estimation of the electrical conductivity of the metal deposit. The higher the order of the resonance modes of these ring resonators is, the higher the Q factor will be. Notably, this electromagnetic model gives an equivalent value of the conductivity of a smooth metal layer at different frequencies and hypothesizes that the metal layer is uniform in thickness. However, the quality factor of this resonator is a good indicator of the quality of the metal layer, particularly when specific sintering treatments are used to improve the electrical conductivity of the metal layer and the planar resonator quality factor.

Furthermore, the conductivity extracted from an equivalent smooth metal layer decreases as the frequency increases. These phenomena are studied in [36, 37] to characterize and quantify the losses introduced by the dielectric metal interface. In these works, more information is given to explain why conductor losses increase with the frequency. The work in [36] explains more particularly through equivalent models that the conductor losses increase with the frequency, particularly when the skin depth becomes small compared to the metal surface roughness.

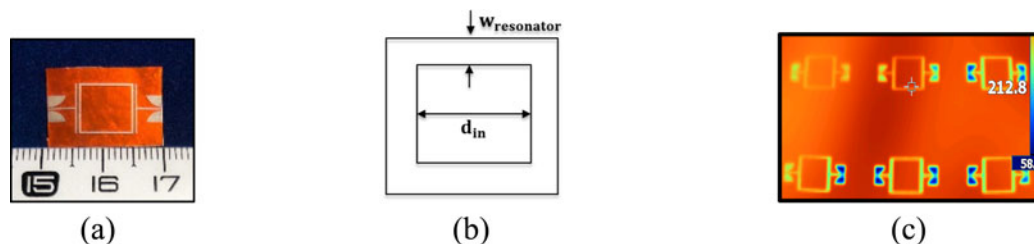


Fig. 2. Silver ring resonator printed with inkjet on a polyimide substrate (a), representation of the dimensions of the sample (b), and thermal image of the samples during drying on the hot plate (c)[31].

Table 1. Polyimide substrate characterization at three frequencies.

f_r (GHz)	ϵ_r	$\text{tg } \delta$
7	3.35 ± 0.035	$0.99 \times 10^{-2} \pm 4.13 \times 10^{-4}$
14	3.29 ± 0.050	$1.06 \times 10^{-2} \pm 3.75 \times 10^{-4}$
21	3.23 ± 0.036	$1.13 \times 10^{-2} \pm 2.68 \times 10^{-4}$

Experimental results. After several preliminary tests with IPL sintering, it was deduced that distributing the energy of the lamp over several pulses avoids continuously heating the sample and an accumulation of heat that can severely damage the polymer substrate. As the pulse time decreases, the power of the IPL light increases and can cause cracks and ablations in the metal layer. Thus, sending the maximum energy of the lamp ($E = 2433$ J/pulse) at a distance of less than 5 cm must be avoided so that no ablations of the metal layer or deformations of the substrate occur.

The most relevant IPL sintering parameters, which allow a substantial improvement in the quality factor and the electrical conductivity, are presented in Table 2.

Figure 4 illustrates the measured transmission coefficients (S_{21}) of the resonators before and after IPL sintering. The measurements of the quality factor at the three resonant frequencies, as well as the estimated values of the equivalent electrical conductivity, are presented in Table 3. After sintering,

an improvement in the quality factors was observed, which is justified by the refinement of the transmission peaks. This improvement in the transmission level is a direct consequence of a substantial optimization of the conductivity of the metal layer. Samples 1–3 do not show substantial physical damage, but sample 4 presents minor damage and therefore changes in its final dimensions after IPL sintering. The latter changes induced a frequency behavior that is slightly different for its resonance frequencies and made them shift towards lower frequencies after IPL sintering, contrary to the expected behavior (Figs 3(a) and 4, samples 1 to 3). The final quality factor and its rate of improvement are related to the initial value of the quality factor, which varies between samples because of the drying inhomogeneity on the hot plate, as shown in Fig. 2(c). The most relevant results are obtained from the IPL sintering parameters for the two-pulse sintering case, which corresponds to sample 2.

The electrical conductivity at each resonance frequency is extracted considering the microwave characteristics of the PI substrate (permittivity and loss tangent) at each resonance frequency. Figure 5 shows top and crosscut SEM images of the metal layers before and after IPL sintering. After drying on the hot plate, the metal nanoparticles are small with rare grain boundaries. After IPL sintering, grain boundaries are created between the nanoparticles, inducing a conductive path with less porosity in the microstructure, which is justified by the improved electrical conductivity of the metal deposit after IPL treatment [38].

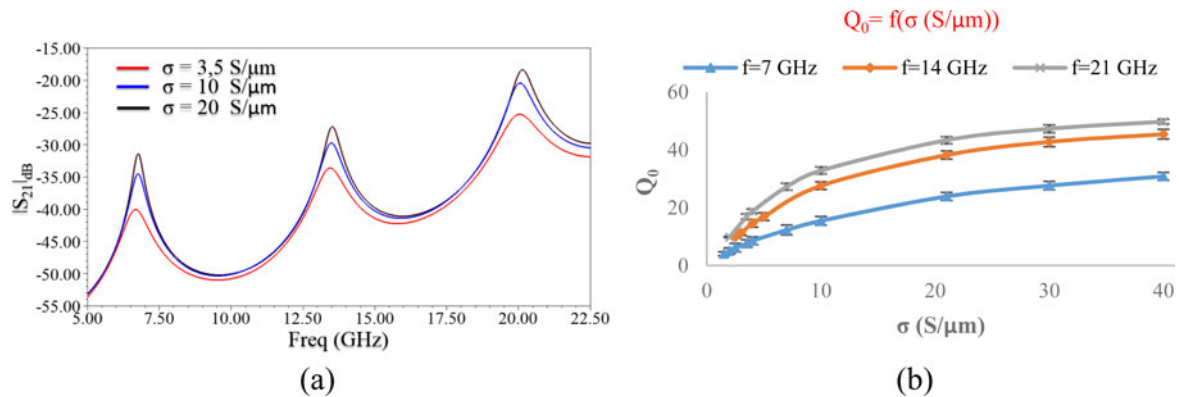


Fig. 3. Effect of the electrical conductivity of the metal deposit on the simulated resonator transmission coefficient (a) and evolution of the quality factor of the printed silver resonator as a function of the conductivity for its first three resonant frequencies (b) (HFSS simulation).

Table 2. IPL sintering parameters used for the optimization of the electrical conductivity.

Samples	Voltage (V)	Number of pulses	d_{Lamp} (cm)	T_{ON} (μ s)	T_{OFF} (μ s)	Energy density (J/pulse)
1	2500	1	5	7000	—	Pulse 1 1690
2	2500	2	5	1400	1400	Pulse 1 1274 Pulse 2 371
3	2500	3	5	875	875	Pulse 1 986 Pulse 2 445 Pulse 3 200
4	3000	3	10	875	875	Pulse 1 1420 Pulse 2 641 Pulse 3 289

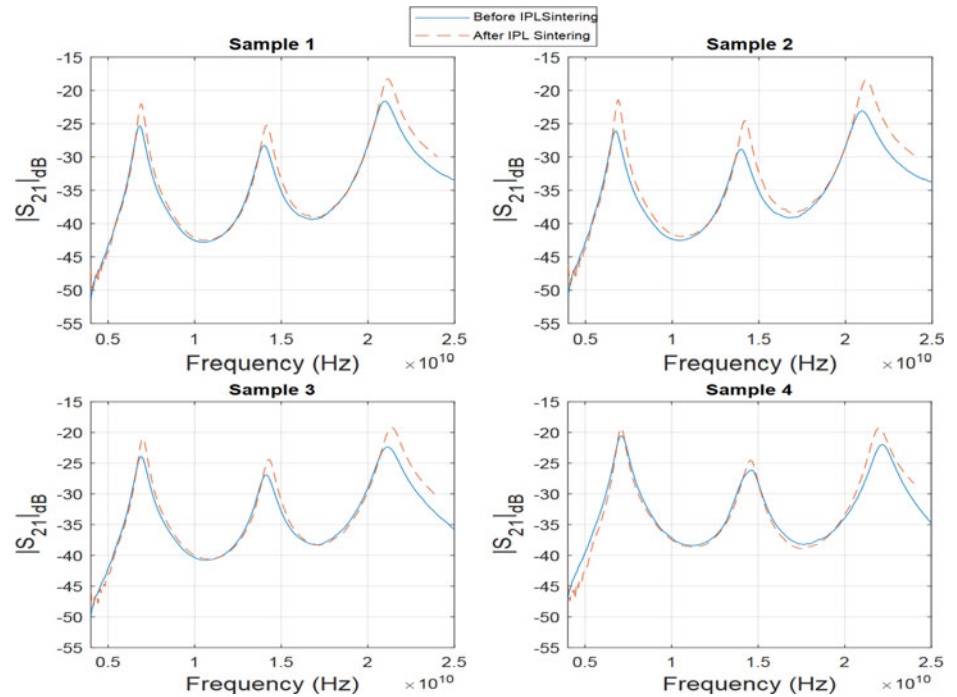


Fig. 4. Measurements of resonator S_{21} before and after IPL sintering for samples 1, 2, 3, and 4.

Table 3. Quality factor measurements before and after sintering and extraction of estimated microwave conductivity values.

		Frequency	7 GHz	14 GHz	21 GHz
Sample 1	Before sintering	Q_0	11.9 ± 0.64	16.2 ± 0.53	18.9 ± 0.55
		σ (S/ μm)	6 ± 0.14	4.56 ± 0.12	3.8 ± 0.11
	After sintering	Q_0	16.7 ± 0.70	22.7 ± 0.6	25.6 ± 0.50
		σ (S/ μm)	11.3 ± 0.18	7.11 ± 0.15	5.9 ± 0.15
		% improvement of Q_0	40%	40%	35%
Sample 2	Before sintering	Q_0	10.6 ± 0.35	14.5 ± 0.51	16.3 ± 0.19
		σ (S/ μm)	5 ± 0.15	3.98 ± 0.12	3.14 ± 0.11
	After sintering	Q_0	17 ± 0.74	22.5 ± 0.80	24.8 ± 0.50
		σ (S/ μm)	11.9 ± 0.25	7.02 ± 0.12	5.61 ± 0.15
		% improvement of Q_0	60%	55%	52%
Sample 3	Before sintering	Q_0	10.3 ± 0.32	14.8 ± 0.51	16.4 ± 0.19
		σ (S/ μm)	4.8 ± 0.14	4.08 ± 0.13	3.16 ± 0.11
	After sintering	Q_0	15 ± 0.73	21.1 ± 0.75	22 ± 0.45
		σ (S/ μm)	9.26 ± 0.19	6.4 ± 0.11	4.69 ± 0.12
		% improvement of Q_0	46%	43%	34%
Sample 4	Before sintering	Q_0	10.7 ± 0.35	13.2 ± 0.35	17.9 ± 0.55
		σ (S/ μm)	5.13 ± 0.16	3.54 ± 0.12	3.54 ± 0.11
	After sintering	Q_0	16 ± 0.70	18.6 ± 0.7	23.2 ± 0.52
		σ (S/ μm)	10.3 ± 0.19	5.41 ± 0.12	5.1 ± 0.12
		% improvement of Q_0	50%	41%	30%

Processing of aerosol jet printed and oven-dried samples

In this section, we again consider samples that are square ring resonators on the PI substrate but printed this time by AJP [10]. The average thickness of the printed silver ink is $0.8 \mu\text{m}$,

and the resonator sizes are $W_{\text{resonator}} = 225 \mu\text{m}$ and $d_{\text{in}} = 8.22 \text{ mm}$. In this case, their first three resonances are at 5, 10, and 15 GHz. After printing, the test patterns were dried in an oven to avoid the constraint of inhomogeneous drying of the samples

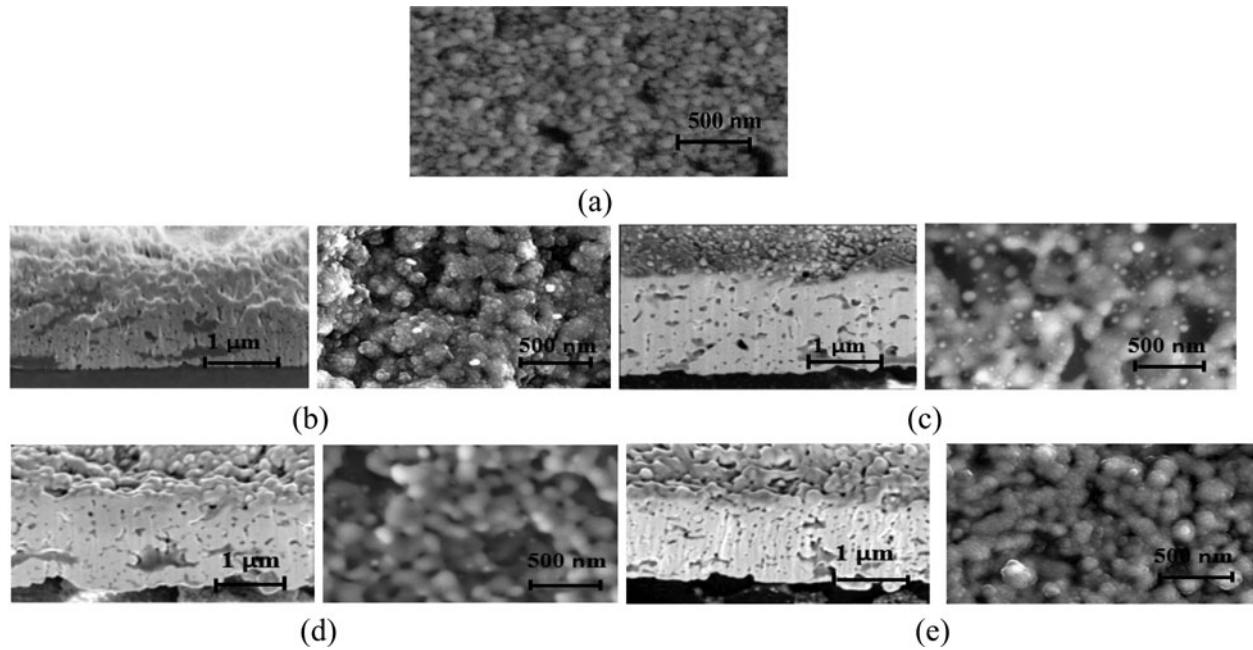


Fig. 5. Top and cross-section SEM images of metal deposits after drying on the hot plate (a, top view only) [31] and after IPL sintering of sample 1 (b), sample 2 (c), sample 3 (d), and sample 4 (e).

Table 4. IPL sintering parameters used for the optimization of the electrical conductivity.

Samples	Voltage (V)	Number of pulses	d_{Lamp} (cm)	T_{ON} (μ s)	T_{OFF} (μ s)	Energy density (J/pulse)	
5	2500	1	5	7000	—	Pulse 1	1690
6	3000	6	10	438	438	Pulse 1	864
						Pulse 2	575
						Pulse 3	383
						Pulse 4	255
						Pulse 5	170
						Pulse 6	114

on the heating plate, as illustrated by the thermal images (Fig. 2(c)) in part A.1. The silver ink was dried following a heating ramp from 30 to 180°C. After this ramp, the samples were heated for 60 min at 180°C. IPL sintering was then applied after this first drying step. Samples S_{21} , unloaded Q factors and extracted equivalent conductivities at microwave frequencies were measured as explained previously. After the ink drying step, which lasted 16 h, IPL was used to improve the conductivity of the conductive deposit. The most relevant IPL sintering parameters used, as well as the characterization of the microwave conductivity, are presented in Tables 4 and 5, respectively.

Figure 6 shows the top SEM images of the metal layer after oven drying and IPL sintering. After sintering in the oven, the nanoparticles started to densify, creating grain boundaries between them. IPL sintering allowed minimization of the pores between the nanoparticles to create a conductive path between the particles. The measured S_{21} values of samples 5 and 6 before and after IPL sintering are similar to the plots presented in Fig. 4.

When the energy of the lamp is divided into several pulses, the energy of the first pulse is absorbed mainly by the upper surface of the film. When the other pulses are applied consecutively, the

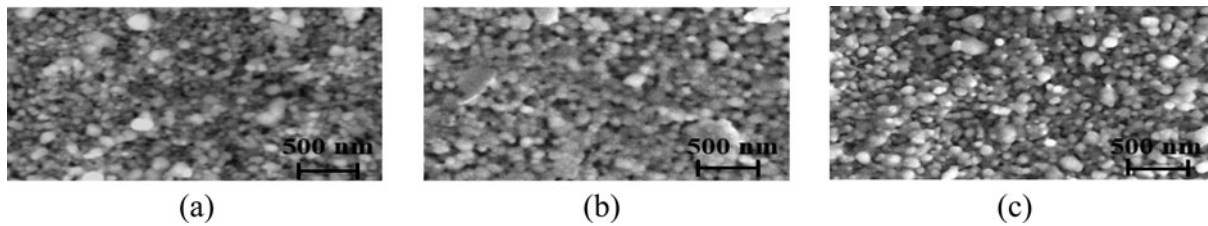
nanoparticles below the surface layer are sintered by heat transfer from the top surface of the metal layer. At the same time, the thermal decomposition of organic additives inside the silver film induces vaporization. However, once the metal layer is formed on the surface of the film, the internal gases are not easily evaporated, which could cause the film to swell during reflow of the surface metal layer in the second or third light irradiation, as explained in [5]. As seen in [31], this result leads to a small dwelling for samples 2 and 3. In sample 4, we notice that burnt areas are at the level of the metal layer because of the extremely short time between the pulses ($T_{off} = 438 \mu$ s), which did not allow sufficient cooling time for the metal deposit. The observed local deformation does not substantially change the microwave behavior of the resonators. However, complementary tests are needed to check the adhesion quality of the silver layer on the PI substrate.

Laser sintering

Unlike most alternative sintering techniques (hot plate, oven, UV, or IR sintering), laser sintering is a selective, fast, and localized sintering process. It consists of sintering the metal deposit

Table 5. Quality factor measurements before and after sintering and extraction of estimated microwave conductivity values.

		Frequency	5 GHz	10 GHz	15 GHz
Sample 5	Before sintering	Q_0	9.9 ± 0.42	14.3 ± 0.45	18.3 ± 0.48
		σ (S/ μm)	11 ± 0.30	8.37 ± 0.12	7.6 ± 0.15
	After sintering	Q_0	14 ± 0.39	19.8 ± 0.50	24.4 ± 0.50
		σ (S/ μm)	19.4 ± 0.35	13.4 ± 0.12	11.8 ± 0.14
		% improvement of Q_0	41%	38.5%	33%
Sample 6	Before sintering	Q_0	13 ± 0.37	19.5 ± 0.50	24.8 ± 0.50
		σ (S/ μm)	17.1 ± 0.40	13.1 ± 0.12	12.2 ± 0.11
	After sintering	Q_0	14.5 ± 0.39	22.2 ± 0.55	27.3 ± 0.53
		σ (S/ μm)	20.6 ± 0.30	16 ± 0.15	14.4 ± 0.14
		% improvement of Q_0	11.5%	14%	10%

**Fig. 6.** SEM images of the silver surface after drying (a) and after IPL sintering (b; samples 5 and c; sample 6).**Table 6.** Summary of the results of three laser sintering techniques.

		Frequency	5 GHz	10 GHz	15 GHz
Sample 7: Hatching technique	Before sintering	Q_0	8.7 ± 0.18	11.6 ± 0.02	15 ± 0.04
		σ (S/ μm)	5.37 ± 0.43	3.48 ± 0.53	3.83 ± 0.12
	After 24 passes	Q_0	13 ± 0.39	18.4 ± 0.06	20.5 ± 0.08
		σ (S/ μm)	9.23 ± 0.35	6.3 ± 0.59	6.48 ± 0.39
		% improvement of Q_0	50%	59%	37%
Sample 8: Rectangle technique	Before sintering	Q_0	7.8 ± 0.15	10.3 ± 0.04	11.5 ± 0.03
		σ (S/ μm)	4.64 ± 0.42	3.11 ± 0.4	2.75 ± 0.12
	After 40 passes	Q_0	13 ± 0.39	17.2 ± 0.11	17.3 ± 0.06
		σ (S/ μm)	9.23 ± 0.35	5.74 ± 0.5	5 ± 0.4
		% improvement of Q_0	67%	67%	51%
Sample 9: Square technique		Frequency	7 GHz	14 GHz	21 GHz
	Before sintering	Q_0	7.3 ± 0.20	10.9 ± 0.32	12.1 ± 0.19
		σ (S/ μm)	3.28 ± 0.14	2.81 ± 0.10	2.41 ± 0.10
	After 40 passes	Q_0	11 ± 0.30	16.39 ± 0.45	18 ± 0.48
		σ (S/ μm)	5.87 ± 0.13	4.72 ± 0.12	3.81 ± 0.12
		% improvement of Q_0	51%	50%	49%

using a laser beam at a fixed wavelength in continuous or pulsed mode.

In our research, an infrared laser that sends pulses at the frequency $f = 40$ kHz at $\lambda = 1064$ nm is used to sinter similar inkjet printed ring resonators. The laser was defocused to provide a

spot diameter equal to $100 \mu\text{m}$ (using a focal distance of 3 mm) and to avoid damage to the polymer substrate. The scanning speed of the laser can be set between 1 and 100 mm/s, and its maximum output power is 20 W by selecting the intensity of the laser current source (0–50 A).

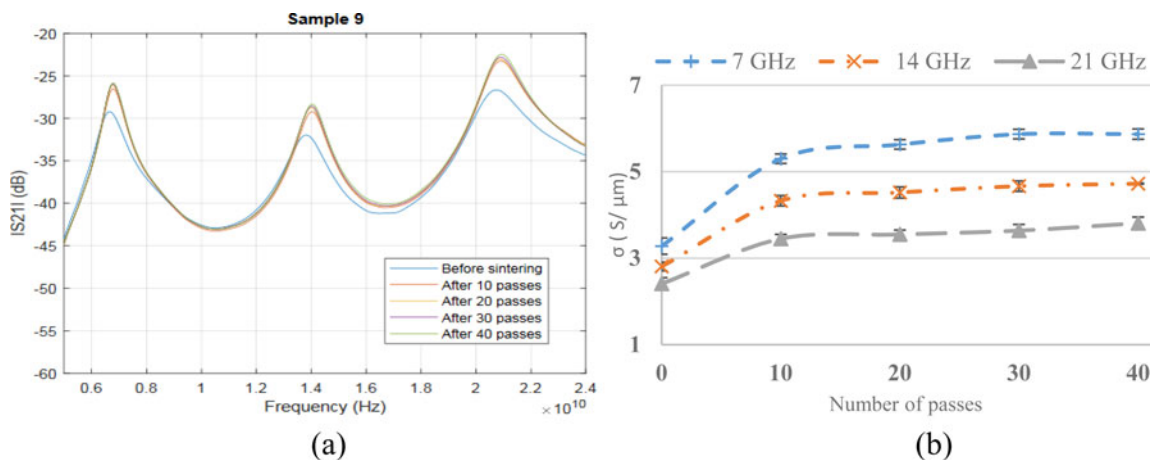


Fig. 7. Measurements of sample 9 before and after 40 laser passes (a) and improvement of the conductivity according to the number of laser passes (b).

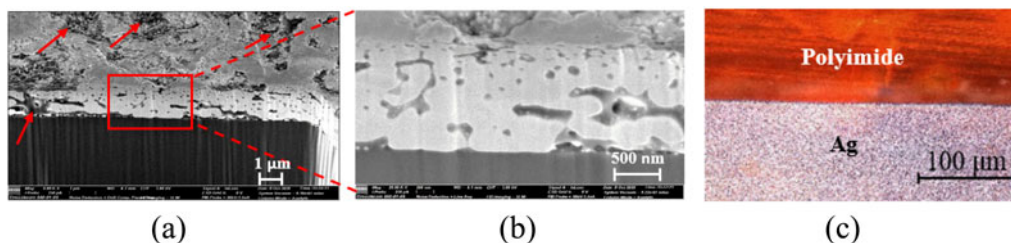


Fig. 8. Cross-section SEM images of the metal layer after 40 laser passes (a, b) and microscopic top image of the edge of the resonator after the laser passes (c).

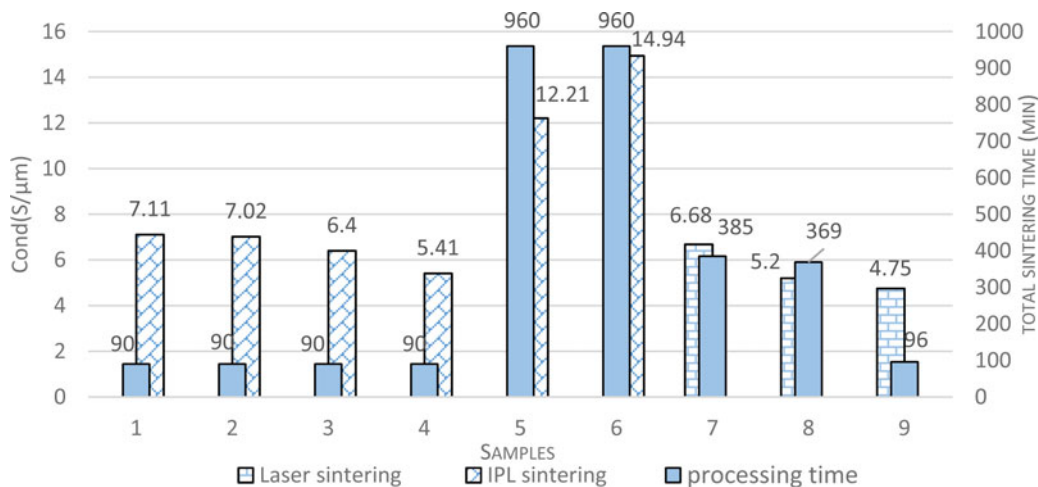


Fig. 9. Final electrical conductivity of the metal deposit after laser or IPL treatment as a function of the total sintering time at $f = 14$ GHz.

Description of the sintering methods

The laser sintering of inkjet printed resonators has already been tested with two methods [32], and a third method is proposed in this section.

After printing the samples, they were dried at 200°C for 6 h on a hot plate to evaporate the solvents present in the ink.

The three selective sintering techniques consist of passing the laser only over the metal layer to increase its conductivity without damaging the polymer substrate near and beneath it.

The common point between these three techniques is the passage of the laser beam on or near the edges of the resonator where

there is a maximum strength of magnetic fields to provide excellent current conductivity. The first two techniques, i.e. the hatching and rectangular techniques, are described in [32].

Considering the noticeably long total sintering time (drying and laser sintering) for these two previous techniques, we intend to reduce the drying time on the hot plate to 90 min, as well as the laser sintering time, by proposing a third technique that we call the square technique. It is inspired by [35] and consists of scanning the sample with the laser passing on the edges of the resonator. For the other two sintering methods, the laser beam was defocused to avoid damage to the polymer substrate. For the

square method, we used 8% laser power with a scanning speed of 10 mm/s. The sintering time is 6 min after 40 laser passes.

Experimental results

Table 6 provides the measured unloaded Q factors and the extracted equivalent conductivity before and after the laser sintering step with the three proposed techniques (hatching, rectangle, and square).

S parameter measurements and equivalent conductivity extraction are performed for 10, 20, 30, and 40 passes of the laser with the square technique (Fig. 7(a)).

The main improvement in the conductivity is after the first 10 passes because, as shown in Fig. 7(b), the electrical conductivity of the deposit becomes saturated.

According to the microstructural distribution (MD), we noticed that the nanoparticles melted and created grain boundaries between themselves, which made it possible to build conductive paths (Figs 8(a) and 8(b)). Because the laser is localized sintering, the MD is not homogeneous over the entire metal deposit, which is illustrated by the red arrows and can be represented as traps for the nanoparticles.

Microscopic images of the sample after the laser treatment (Fig. 8(c)) show no ablation and no damage to the polymer substrate or the metal layer. Therefore, laser sintering can be considered a localized sintering technique that improves the electrical conductivity without damaging the deposit if the proper lasing parameters are applied.

Table 6 summarizes the improvement of the quality factor and equivalent electrical conductivity extraction of the metal deposit of the resonators before and after each laser sintering technique.

The three sintering techniques allow a substantial improvement of the quality factor and electrical conductivity. The hatching technique allows the entire metal surface to be sintered but with a long sintering time (25 min), and the rectangle technique achieves almost identical quality factor values as those of the hatching technique in less treatment time (9 min). The square technique represents the trade-off between improving the final quality factor and reducing the total sintering time (6 min).

Because extractions were performed at different frequencies, our conclusions are based on the data that are used to estimate the conductivity of each case at 14 GHz.

Figure 9 presents the final electrical conductivity of the metal deposit at $f = 14$ GHz after the IPL or laser treatment, considering the total treatment time (drying and sintering). Note that to achieve high conductivity values ($\sigma > 12$ S/ μm , typically), the total treatment time must be long (16 h) and to reduce the treatment time (~ 90 min), the final equivalent conductivity is ~ 3.8 – 7.1 S/ μm .

Conclusion

To improve the low conductivity of a given silver ink (3–4.5 S/ μm) by improving the deposit conductivity, two sintering techniques have been studied. Accompanied by detailed microscopic views, unloaded Q factor and equivalent conductivity measurements between 5 and 21 GHz, a study of microwave ring resonator samples was performed for different sintering treatments to determine the strengths and weaknesses of each method.

A maximum equivalent electrical conductivity of 14.49 S/ μm after IPL sintering and of 6.5 S/ μm [32] after laser sintering are obtained at $f = 14$ GHz. Because of these unconventional sintering methods, the unloaded Q factors of silver-printed planar resonators show an improvement of up to +55% (with IPL sintering).

For IPL sintering, this technique distributes the energy emitted by the lamp evenly over the metal deposit. It can treat many metal patterns printed on a substrate at the same time. In addition, the extremely short duration (ms) of the light pulses and the width of their spectrum covering the UV, visible, and IR regions (190–1100 nm) allow it to treat all types of metals and substrates. The ratio between this quick sintering step (a few ms) that follows a conventional drying step (hot plate or oven) and the percentage of improvement of the Q factor of the printed planar resonators at microwave frequencies is excellent.

Laser sintering is a relevant alternative technique. It is a localized annealing step in which the laser can selectively sinter printed metal patterns without damaging the underlying polymer substrate or the nearby components. Lasing times between 6 and 25 min are required depending on the selected lasing strategy, which leads to an improvement of the planar resonator unloaded Q factor of up to +51% at 14 GHz. As a direct consequence, if we consider a fourth-order Chebyshev filter made with these resonators, having a central frequency of 14 GHz, a bandwidth of 2.8 GHz and a return loss of 20 dB, the proposed sintering techniques would provide an improvement of its insertion losses of up to 2.5 dB.

Therefore, the use of these sintering techniques in the field of printed electronics, particularly for sintering printed microwave planar components on low melting temperature polymer substrates, seems to be a relevant, complementary technique to conventional methods. For our future works, we will consider other polymer substrates, such as PEEK ($t_g = 152^\circ\text{C}$), which is widely used in the aeronautics domain, over a broader range of passive components, such as microwave filters, transmission lines (microstrip, CPW), or antennas.

Acknowledgements. The authors thank their colleagues from the Institute for Research on Ceramics (IR CER, Limoges) and, more specifically, Mr. Pierre Carles for his great support with the SEM images of the metal layers.

References

- Borghetti M, Cantù E, Sardini E and Serpelloni M (2020) Future sensors for smart objects by printing technologies in industry 4.0 scenario. *Energies* **13**, Art. no. 22. doi: 10.3390/en13225916
- Cruz S, Rocha I and Viana J (2018) 'Printing Technologies on Flexible Substrates for Printed Electronics'.
- Seifert T, Sowade E, Roscher F, Wiemer M, Gessner T and Baumann RR (2015) Additive manufacturing technologies compared: morphology of deposits of silver ink using inkjet and aerosol jet printing. *Industrial & Engineering Chemistry Research* **54**, 769–779.
- Baron S (2015) 'Flexible polymer for X-band electrically tunable patch antenna: design and characterizations', Theses, Université de Nantes.
- Mitra KY, Alalawe A, Voigt S, Boeffel C and Baumann RR (2018) Manufacturing of all inkjet-printed organic photovoltaic cell arrays and evaluating their suitability for flexible electronics. *Micromachines* **9**, Art. no. 12. doi: 10.3390/mi9120642
- Rao Balakrishnan S and Asri M (2014) Conventional photolithography and process optimization of pattern-size expansion technique for nanogap biosensor fabrication. *Advanced Materials Research* **832**, 89–94.
- Abdelghani A (2018) 'Microwave gas sensor based on carbon nanotubes, printed by inkjet technology', Doctoral thesis, Limoges.
- Macuri CAP 'Design of radio-frequency gas sensors based on carbon nanotubes and inkjet printing', p. 276.
- Lee H, Seo S, Yun K, Joung JW, Oh I and Yook J (2008) 'RF Performance of CPW transmission line fabricated with inkjet printing technology', in *2008 Asia-Pacific Microwave Conference*, Dec. 2008, pp. 1–4, doi: 10.1109/APMC.2008.4958022.
- Delage A (2019) 'Aerosol technology applied to 3D integration and microwave components', Doctoral thesis, Limoges.

11. Florent G 'Additive manufacturing of electroactive materials for mechatronics applications', p. 134.
12. Hu A, Guo JY, Alarifi H, Patane G, Zhou Y, Compagnini G and Xu CX (2010) Low temperature sintering of Ag nanoparticles for flexible electronics packaging. *Applied Physics Letters* **97**, 153117.
13. Minari T, Kanehara Y, Liu C, Sakamoto K, Yasuda T, Yaguchi A, Tsukada S, Kashizaki K and Kanehara M (2014) 'Room-Temperature Printing of Organic Thin-Film Transistors with π -Junction Gold Nanoparticles – Minari – 2014 – Advanced Functional Materials – Wiley Online Library'.
14. Joo S-J, Hwang H-J and Kim H-S (2014) Highly conductive copper nano/microparticles ink via flash light sintering for printed electronics. *Nanotechnology* **25**, 265601.
15. Xu H, Tang X, Sun H, Zhao H and Li M (2017) 'Conductivity of silver and copper film printed by particle-free reactive inks', in *2017 18th International Conference on Electronic Packaging Technology (ICEPT)*, Harbin, China, Aug. 2017, pp. 1470–1473, doi: 10.1109/ICEPT.2017.8046713.
16. Sarkar SK, Gupta H and Gupta D (2016) 'Flash light sintering of silver ink for inkjet printed organic thin film transistor on flexible substrate', in *2016 3rd International Conference on Devices, Circuits and Systems (ICDCS)*, Mar. 2016, pp. 68–72, doi: 10.1109/ICDCSyst.2016.7570627.
17. Wang Z, Zhao T, Liang X, Zhu P and Sun R (2017) 'A low cost method to synthesize silver nanoparticles for the screen printing conductive inks', in *2017 18th International Conference on Electronic Packaging Technology (ICEPT)*, Aug. 2017, pp. 1121–1124, doi: 10.1109/ICEPT.2017.8046638.
18. Moon K-S, Dong H, Maric R, Pothukuchi S, Hunt A, Li Y and Wong CP (2005) Thermal behavior of silver nanoparticles for low-temperature interconnect applications. *Journal of Electronic Materials* **34**, 168–175.
19. Ndayishimiye A 'On a new low-temperature ceramic sintering process: hydrothermal sintering. Development and mechanistic approach', p. 213.
20. Herring C (1950) Effect of change of scale on sintering phenomena. *Journal of Applied Physics* **21**, 301–303.
21. Rieger J (2000) 'Glass Transition Temperature (T_g) of Plastics - Definition & Values'. Available at <https://omnexus.specialchem.com/polymer-properties/properties/glass-transition-temperature>.
22. Khan S, Dahiya R and Lorenzelli L (2014) Technologies for printing sensors and electronics over large flexible substrates: a review. *IEEE Sensors Journal*. doi: 10.1109/JSEN.2014.2375203.
23. Baudino O 'Photonic sintering of printed lines based on nanoparticles: optimization of electrical and mechanical properties for the interconnection of integrated circuits on flexible substrates', p. 191.
24. Lopes AJ, Lee IH, MacDonald E, Quintana R and Wicker R (2014) Laser curing of silver-based conductive inks for *in situ* 3D structural electronics fabrication in stereolithography. *Journal of Materials Processing Technology* **214**, 1935–1945.
25. Kim M-K, Hwang JY, Kang H, Kang K, Lee S-H and Moon S-J (2009) 'Laser sintering of the printed silver ink', in *2009 IEEE International Symposium on Assembly and Manufacturing*, Nov. 2009, pp. 155–158, doi: 10.1109/ISAM.2009.5376912.
26. Kim M-K, Kang H, Kang K, Lee S-H, Hwang JY, Moon Y and Moon S-J (2010) 'Laser sintering of inkjet-printed silver nanoparticles on glass and PET substrates', in *10th IEEE International Conference on Nanotechnology*, Aug. 2010, pp. 520–524, doi: 10.1109/NANO.2010.5697913.
27. Lee DJ, Park SH, Jang S, Kim HS, Oh JH and Song YW (2011) Pulsed light sintering characteristics of inkjet-printed nanosilver films on a polymer substrate. *Journal of Micromechanics and Microengineering* **21**, 125023.
28. Kang JS, Ryu J, Kim HS and Hahn HT (2011) Sintering of inkjet-printed silver nanoparticles at room temperature using intense pulsed light. *Journal of Electronic Materials* **40**, 2268.
29. Krebs FC (2009) Fabrication and processing of polymer solar cells: a review of printing and coating techniques. *Solar Energy Materials and Solar Cells* **93**, 394–412.
30. Sun Y and Rogers JA (2007) Inorganic semiconductors for flexible electronics. *Advanced Materials* **19**, 1897–1916.
31. Hajjaji CE, Delhote N, Verdeyme S, Piechowiak M and Durand O (2021) 'Optimization of the conductivity of microwave components printed by inkjet on polymeric substrates by photonic sintering', in *2020 50th European Microwave Conference (EuMC)*, Jan. 2021, pp. 380–383, doi: 10.23919/EuMC48046.2021.9338007.
32. Hajjaji CE, George J, Lmansouri S, Delhote N, Verdeyme S, Baillargeat D, Piechowiak M and Durand O (2019) 'Optimizing the conductivity of ink-jet printed microwave components on polymer substrates by laser sintering', in *2019 49th European Microwave Conference (EuMC)*, Oct. 2019, pp. 778–781, doi: 10.23919/EuMC.2019.8910768.
33. 'Flash lamp Eg&G.pdf', Available at <https://www.flashlamps-vq.com/CatalogueVQF.pdf>.
34. Mittal KL (2005) *Polyimides and Other High Temperature Polymers: Synthesis, Characterization and Applications*, held in Orlando, December 17-19, 2003
35. Rojas-Nastrucci EA (2017) Characterization and modeling of K-band coplanar waveguides digitally manufactured using pulsed picosecond laser machining of thick-film conductive paste. *IEEE Transactions on Microwave Theory and Techniques* **65**, 3180–3187.
36. Méndez-Jerónimo G, Sejas-García SC and Torres-Torres R (2018) Modeling and parameter extraction for the metal surface roughness loss effect on substrate integrated waveguides from S-parameters. *IEEE Transactions on Microwave Theory and Techniques* **66**, 875–882.
37. Ding R, Braunisch H, Tsang L and Chang W (2012) 'Simulation and measurement correlation of random rough surface effects in interconnects', in *2012 IEEE 21st Conference on Electrical Performance of Electronic Packaging and Systems*, Oct. 2012, pp. 272–275, doi: 10.1109/EPEPS.2012.6457894.
38. Greer JR and Street RA (2007) Thermal cure effects on electrical performance of nanoparticle silver inks. *Acta Materialia* **55**, 6345–6349.



Chaimaa El Hajjaji received a master's degree in High Technologies, Electronics, and Photonics from the University of Limoges, France, in 2018. She is now a Ph.D. candidate with the MACAO team in the XLIM Laboratory in collaboration with the Centre for Technology Transfers in Ceramics (CTTC) at Limoges. Her research interests mainly focus on the design of microwave components and the improvement of their performance using emerging sintering techniques.



Dr. Nicolas Delhote received his Ph.D. in 2007 from the University of Limoges, France. He is the head of the MACAO research group dedicated to the design, optimization and fabrication of microwave components. His main activities are related to advanced manufacturing technologies (additive manufacturing) and materials and to the design and optimization of passive microwave components (filters, power dividers, etc.) for space and defence applications.



Dr. Serge Verdeyme received a Ph.D. from the University of Limoges, Limoges, France, in 1989. He is currently a professor at XLIM, Laboratory of the CNRS and the University of Limoges, and works in the RF System Department. His primary field of interest concerns the design and optimization of microwave components.



Dr. Malgorzata Anna Piechowiak has got double Ph.D. in Materials Science and Ceramic Processing at the University of Limoges (France) and Physics of Matter at the University of Genoa (Italy) in 2011. She has over 8 years of international research experience in ceramic engineering (powder synthesis, formulation of dispersions and pastes, additive manufacturing, film deposition, etc.). Presently, she occupies R&D manager position in the Centre for Technology Transfers in Ceramics (CTTC) and works on projects linked with the development of

ceramic-based functional parts by additive manufacturing processes such as binder jetting, aerosol jet, or inkjet printing.



Eng. Laurence Boyer has a technical background in chemistry and materials. She has 15 years of experience in the ceramic industry acquired in France, Spain in the UK. She joined the Centre for Technology Transfers in Ceramics (CTTC) at Limoges in 2018 as the head of Resourcing and Technologies Department for defining and monitoring the collaborative research and scientific resourcing

activities. She is in charge of a team composed of doctors, engineers, and technicians working on the development of new materials and manufacturing processes of technical ceramics. She also uses her international

experience to set up and carry out European projects and the dissemination of results.



Dr. Olivier Durand received his Ph.D. at the University of Limoges in 2006 after fundamental research work on the crystallography of tellurium oxides. After a 3-year postdoctoral fellowship on ceramic processes, he joined the Centre for Technology Transfers in Ceramics (CTTC) at Limoges in 2009, working as a project manager for 5 years and then as the Materials and Processes Department manager

for 3 years. He has registered one patent and has collaborated on five research articles. He is currently the CEO of CTTC, a Research and Technology Organization specializing in ceramic materials and the processes thereof.